https://doi.org/10.5194/egusphere-2026-3094
Preprint. Discussion started: 23 June 2026

Spatiotemporal variations of carbon-water-hydraulic risk for *Pinus tabuliformis* L. Plantations on the Loess Plateau under Future Climate Change

Tianqi Guo[1], Zhongdian Zhang[3,4], Rui Liu[1], Xiaofei Wu[5], Xinmei Liu[1], Chenyi Ju[2], and Mingbin Huang[2*]

[1] College of Natural Resources and Environment, Northwest A & F University, Yangling 712100, China

[2] State Key Laboratory of Soil Erosion and Dryland Farming on the Loess Plateau, College of Soil and Water Conservation Science and Engineering, Northwest A & F University, Yangling 712100, China

[3] School of Geographic Sciences, Xinyang Normal University, Xinyang 464000, China

[4] Henan Key Laboratory for Synergistic Prevention of Water and Soil Environmental Pollution, Xinyang Normal University, Xinyang 464000, China

[5] Shaanxi Academy of Forestry, Xi'an, 710082, China

*Corresponding author: Mingbin Huang, hmbd@nwsuaf.edu.cn

https://doi.org/10.5194/egusphere-2026-3094
Preprint. Discussion started: 23 June 2026

Abstract. As a native perennial tree, *Pinus tabuliformis* L. (PT) has been widely planted on the Chinese Loess Plateau for ecological restoration. However, climate change impacts on water resources will poses a new challenge for sustainability of restored ecosystems. To clarify the plantations carbon sequestration and water consumption, as well as their underlying physiological mechanisms, this study coupled the integrated BBGC-Sperry model with CMIP6 meteorological data under SSP126, SSP245, and SSP585. Daily transpiration, soil water content, and leaf water potential, along with multi-site total growing-season transpiration and aboveground biomass data, were used to validate the BBGC-Sperry model. The validated model simulated the dynamics of NPP, actual evapotranspiration (ET) and annual average percentage loss of whole-plant hydraulic conductivity (APLK) for PT plantations at 130 meteorological stations on the Loess Plateau. We integrated a "carbon-water-hydraulic risk index" (CWHRI) based on NPP, ET, and drought-induced mortality risk probability (DMRP) to assess ecosystem sustainability. These simulations covered the baseline period (2000-2024) and three future periods (2025-2049, NFP; 2050-2074, MFP; and 2075-2099, FFP). The results indicate that the mean NPP will decrease by 4%-27% except in the FFP under the SSP585 while the mean ET and APLK will increase by 0.05%-61% and 13%-84%, respectively. The CWHRI will decline by 23%-44%, driven directly by NPP and indirectly by water-related environmental factors. The spatial dynamics of CWHRI will decline from southeast to northwest. These findings indicate the rising DMRP of PT plantations will threaten the sustainability of restored ecosystems on the Loess Plateau in the future.

https://doi.org/10.5194/egusphere-2026-3094
Preprint. Discussion started: 23 June 2026

Keywords: Climate change; BBGC-Sperry model; Net primary productivity; Actual evapotranspiration; Drought-induced mortality risk; The Loess Plateau

https://doi.org/10.5194/egusphere-2026-3094
Preprint. Discussion started: 23 June 2026

1 Introduction

Plantations play a vital role in ecological restoration (Fan et al., 2024; Chen et al., 2025) and significantly contributes to global biogeochemical cycles (Piao et al., 2020).The monoculture plantations can quickly boost regional ecosystem productivity and carbon storage (Li Q. et al., 2025). However, against the backdrop of rising global temperatures and shifting precipitation patterns, the frequent occurrence of compound drought events poses an increasingly severe threat to the physiological processes of forest plantations, while triggering a series of negative hydrological feedback effects, especially in ecologically fragile regions (Tang and Chen, 2025; Qi et al., 2025; Zhou et al., 2019; Feng et al., 2016; Brodribb et al., 2020; Ma et al., 2023; Liu et al., 2023; Li Z. et al., 2025). These phenomena have raised concerns about the production, ecological benefits, and drought-induced mortality risk of plantations under the future climate change (Li Q. et al., 2025). Therefore, accurately assessing the response of plantation productivity, evapotranspiration, and drought-induced mortality risk to climate change is a critical prerequisite for developing adaptive management strategies and ensuring ecological security.

Most current regional-scale studies rely on environmental surrogate indicators such as meteorological drought indices, soil moisture, forest net primary productivity (NPP), or remote sensing-based vegetation greenness or productivity models to obtain information on ecosystem or individual plant growth (Jiao et al., 2021; Li et al., 2021; Chen Z. et al., 2024; He et al., 2024; Wang et al., 2025). These traditional assessment methods can characterize ecological functionality macroscopically, but they fail to

https://doi.org/10.5194/egusphere-2026-3094
Preprint. Discussion started: 23 June 2026

capture the critical internal physiological mechanisms underlying tree survival under drought stress, resulting in a gap in understanding of drought-induced mechanisms in forests under climate change. These methodological limitations may lead to overestimate vegetation growth, as plant physiological responses occur faster than canopy changes under drought stress (Tang et al., 2026). Therefore, accurately assessing drought-induced mortality risk at the regional scale can provide a deeper understanding of the security and sustainability of plantation restoration ecosystems.

Currently, investigating the mechanisms of drought-induced tree mortality is daunting due to the complex physiological and ecological processes involved (McDowell et al., 2008, 2022; Arend et al., 2021). A comprehensive drought response mechanism should start from climatic drivers, proceed through the regulation of ecosystem hydrological processes, and ultimately affect the physiological processes of individual trees, thereby determining their mortality probability (McDowell et al., 2022; Ma et al., 2023). At the regional scale, field monitoring is time-consuming and labor-intensive. Therefore, there is an urgent need for models that integrate plant hydraulic and ecological processes. Zhang et al. (2020) developed the eco-hydrological-hydraulic (BBGC-Sperry model) model by coupling a plant hydraulic process model (Sperry model) with a biogeochemical model (Biome-BGC model). This model uses a supply－demand function to overcome the limitations of empirical functions in describing plant water use responses to soil and atmospheric drought. Yan et al.(2022) have successfully used this model to assess the drought-induced mortality risk of *Robinia pseudoacacia* plantations at four meteorological stations across a typical precipitation gradient on the

https://doi.org/10.5194/egusphere-2026-3094
Preprint. Discussion started: 23 June 2026

Loess Plateau. Wu et al. (2026) improved the Penman-Monteith equation, which used in the BBGC-Sperry model for evapotranspiration calculations, enhancing its ability to account for the effects of elevated atmospheric CO_2 on evapotranspiration. This improvement enabled accurate assessment of actual evapotranspiration (ET) in PT plantations on the Loess Plateau. These model improvements and applications provide a solid foundation for assessing the growth dynamics of plantations on the Loess Plateau. However, existing studies have been largely conducted at the site scale, and the application of this model at the regional scale remains to be validated. The improved BBGC-SPERRY model allows for more accurate simulations of key vegetation growth and physiological indicators, including net primary productivity (NPP), evapotranspiration (ET), and the annual average percentage loss of whole-plant hydraulic conductance (APLK). It serves as a reliable tool for revealing the true vulnerability of forests, avoiding systemic misjudgments, and supporting the construction of a “Carbon-Water-Hydraulic Risk Index” (CWHRI) framework.

The Loess Plateau of China is one of the most climate-sensitive regions globally, with a warming rate above the global average and increasing variability in precipitation (Yan et al., 2022). To address land degradation and wind erosion, large-scale afforestation projects, such as the "Grain-for-Green" program, have been implemented in the region since the 1990s (Li et al., 2021). *Pinus tabuliformis* L. (PT) plantations have been widely planted due to their strong drought tolerance and soil fixation capacity, and now form an important regional ecological barrier (Chen et al., 2008). However, PT plantations may lead to a continuous decline in soil water storage due to their high

https://doi.org/10.5194/egusphere-2026-3094
Preprint. Discussion started: 23 June 2026

water consumption, potentially resulting in the formation of stable dry layers (Chen S. et al., 2024). This suggests a potential risk of water imbalance, making tree growth increasingly dependent on unstable precipitation inputs. In some restored areas, PT plantations have already exhibited browning. The uncertainty of future global precipitation patterns is expected to further increase the sensitivity of forest ecosystems to interannual precipitation fluctuations, potentially leading to growth decline, crown dieback, and even tree mortality (Liu et al., 2020). Although the abovementioned risks have received some attention, systematic, mechanistic long-term predictions of the growth dynamics, physiological stress, and spatial variability patterns of PT plantations under multiple future climate scenarios are still lacking.

Therefore, a single-site experiment was conducted in a typical ecological restoration area in Ansai, Shaanxi during the 2024-2025 growing seasons (May 1-September 30). The modified BBGC-Sperry model was validated using measured daily transpiration (T_{day}), midday leaf water potential (Ψ_{md}), and soil water content (SWC), as well as total growing-season transpiration and aboveground biomass data collected from other meteorological stations within the study area. The validated model was used to simulate the spatiotemporal variations of NPP, ET, and APLK at 130 meteorological stations in the study area from 2000 to 2024, and to project future conditions the next 75 years under three Shared Socioeconomic Pathways (SSP126, SSP245, SSP585) from CMIP6. The objectives of this study were to: 1) validate application of the modified BBGC-Sperry model to PT plantations in the study area; 2) reveal spatiotemporal variations of NPP, ET and APLK in PT plantations under climate

https://doi.org/10.5194/egusphere-2026-3094
Preprint. Discussion started: 23 June 2026

change; 3) develop a new index to assess the ecological functionality based on NPP, ET and drought-induced mortality risk (DMRP) and analyze its spatiotemporal variations and influencing factors . The results could provide insights into the adaptability of PT plantations to future climate change and their potential hydrological and physiological vulnerabilities on the Loess Plateau.

2 Materials and methods

2.1 Study area

To control soil and water erosion, large-scale vegetation restoration projects (e.g., the Grain-for-Green Program and the Three-North Shelter Forest Program) were implemented by China's Central Government in this region in the late 1990s (Jia et al., 2017). Native PT, a pioneer species for vegetation restoration, was widely planted due to its drought resistance and is now mainly distributed across Gansu, Shaanxi, and Shanxi provinces on the Loess Plateau (Wang, 2016). Therefore, the green area in Fig. 1 was selected as the simulation area to analyze the growth and drought-induced mortality risk of PT plantations. The study area (102.68-114.55°E, 33.72-40.74°N) is located in the Loess Plateau, covering approximately 380,000 km² (Fig. 1), and encompasses diverse topographic features with hills, gullies, ridges, and basins. The predominant soil types include silt-clay, silt-clay-loam, silt-loam, loam, and sand-loam (Jia et al., 2019). From southeast to northwest, the climate transitions from semi-humid to semi-arid, the mean annual precipitation (MAP) decreases from 700 to 200 mm with 55-78% occurring from June to September, and the mean annual temperature (MAT)

https://doi.org/10.5194/egusphere-2026-3094
Preprint. Discussion started: 23 June 2026

ranges from 14.3 to 3.6 ℃ (Zhang et al., 2024b). The region is characterized by loess deposits ranging from 30 to 200 m thick. Precipitation in the study area is the primary source of recharge and the depth to groundwater is typically between 30 and 100 m (Zhu et al., 2018).

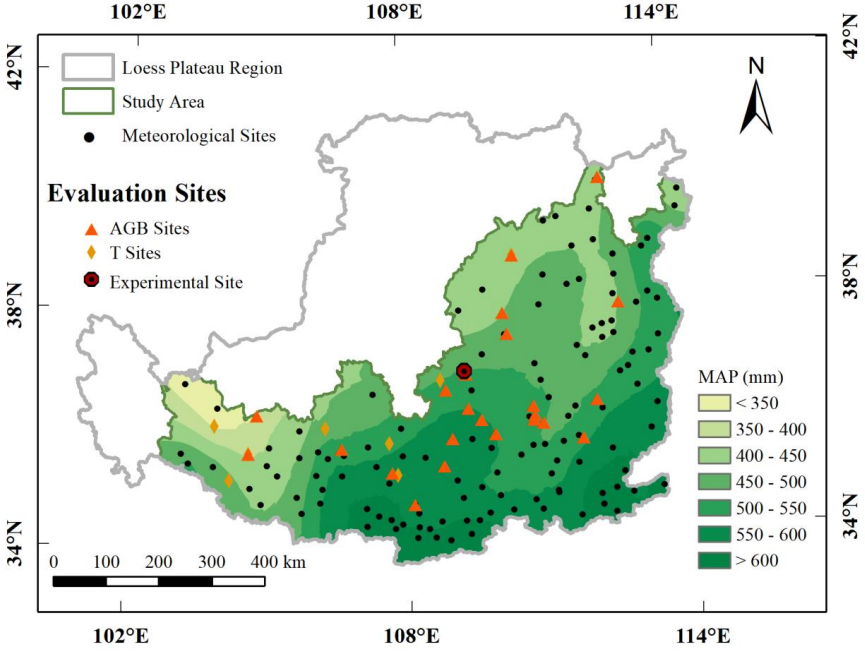

Figure. 1 Map depicting the location of the study area on the Loess Plateau showing the distribution of the 130 modeling sites, nine sites where growing season transpiration (T) data were collected, 27 sites where aboveground biomass (AGB) data were collected, and one experimental site (Ansai).

2.2 BBGC-Sperry model description

BBGC-Sperry is a coupled model integrating the biome biogeochemical cycle model

https://doi.org/10.5194/egusphere-2026-3094
Preprint. Discussion started: 23 June 2026

(Biome-BGC model) with the plant supply-demand hydraulic model (Sperry model). Conventional climate data, soil parameters, and physiological-ecological parameters were incorporated into this model to simulate the dynamic changes in plant hydraulic properties at the daily scale, along with water, carbon, nitrogen, and nitrogen cycling processes. The BBGC-Sperry model is described in detail in previous articles (Zhang et al., 2020; Yan et al., 2022). Here, we briefly outline several key processes.

2.2.1 Water cycle

The only water input to the system occurs through precipitation (rain or snow). The amount of intercepted precipitation depends on the canopy interception coefficient and the leaf area index (LAI). In this model, snowfall reaches the soil surface directly without being intercepted by the vegetation canopy and its sublimation and melt are estimated based on daily air temperature and net solar radiation. Water outflow includes soil evaporation and canopy transpiration (canopy evaporation and evaporation from intercepted water), which are calculated based on modified Penman-Monteith functions with different conductivity types. The modified Penman-Monteith equation takes into account the effect of atmospheric carbon dioxide concentrations on overall surface resistance (Wu et al., 2026). Water transport processes in the soil-plant-atmosphere (SPAC) system were simulated by the Sperry model. The detailed modification of the Sperry model can be found in Zhang et al. (2020). The Sperry model divides the SPAC into serial components of leaves, stems, roots, and rhizosphere. Supply and demand functions are employed to calculate water flux, whole-plant hydraulic conductance (k_{plant}), and the distribution of water potential and hydraulic conductance within the

https://doi.org/10.5194/egusphere-2026-3094
Preprint. Discussion started: 23 June 2026

SPAC system. The vulnerability curves for each component describe the attenuation of hydraulic conductance as water potential decreases, with steady-state flow calculated by integral transformation. The root system is stratified by root density, employing a multidimensional Newton-Raphson iteration method to solve for water potential and water uptake rates within each root layer. Soil moisture movement is simulated using a hydrological submodel based on the Richards equation (Huang et al., 2013).

2.2.2 Carbon and nitrogen cycle

The only addition of C to the system is through photosynthesis. C is removed from the system during all autotrophic (maintenance and growth) processes, heterotrophic (decomposition) processes, and fire or harvest disturbance events. The addition of N to the system is divided into plant N pools and soil N pools. Plant N enters the system through leaf litter, while soil mineralized N is released by the slowest-releasing organic matter, N dry and wet deposition from the atmosphere, and N fixation. Mineralized N is lost from the system by leaching and volatilization. The model uses a two-leaf representation of the canopy to model all canopy photosynthesis, which is based on the enzymatic kinetics of Rubisco in relation to temperature, availability of CO_2, and rate of Rubisco regeneration (Farquhar et al., 1980). For autotrophic respiration, respiration maintenance is modeled using the Q_{10} function of temperature and nitrogen content. Heterotrophic respiration is assumed to be a constant proportion of all new tissue growth (Yan et al., 2022).

2.3 Model evaluation

2.3.1 Hydrological process validation

https://doi.org/10.5194/egusphere-2026-3094
Preprint. Discussion started: 23 June 2026

Daily transpiration (T_{day}), SWC, and midday leaf water potential (Ψ_{md}) during the growing season in PT plantations were used to evaluate the hydrological process of the BBGC-Sperry model. Thus, we established an experimental PT plantation site in Ansai District, Shaanxi Province on May 1, 2024. This area is a key zone for soil and water conservation projects. Field observations were conducted during the 2024 and 2025 growing seasons (1 May to 30 September). The experimental plot had an area of 20 m × 20 m and a tree density of 1600 stems ha^{-1}. Additionally, we measured the sapwood thickness and diameter at breast height of 20 trees near the experimental area using growth cones and vernier calipers and established a regression equation (R^2=0.99) linking diameter at breast height (D) to sapwood area (A_s) in the PT plantation, as follows:

$$A_s=0.34D^{2.095} \quad (1)$$

Stem sap flow sensors were used to measure the sapwood flux density. First, we selected eight representative sample trees based on the distribution of breast height diameter classes. Stem sap flow sensors (Granier type, probe length 10 mm, diameter 1.2 mm, with a 40 mm spacing between the heated probe and reference probe) were uniformly installed at the breast height diameter (1.3 m) to monitor the dynamic changes in sap flow density during the growing season in the PT plantations. During installation, sufficient exposure of the phloem at breast height was ensured. To minimize rainfall and solar radiation effects, sensors were mounted on the shaded side of the trunk. Additionally, the gap between the two probes and the trunk was sealed with petroleum jelly and wrapped in multiple layers of radiation-shielding aluminum

https://doi.org/10.5194/egusphere-2026-3094
Preprint. Discussion started: 23 June 2026

foil. The sensor was connected to a CR1000 datalogger (Campbell Scientific, Logan, UT, USA) and an AM16/32 data expansion board (Campbell Scientific, USA), scanning and collecting data every 30 s while recording hourly averages. The CR1000 datalogger was powered by a 12-volt DC battery and an ES-VR2 voltage regulator, supplemented by solar panels. Based on the measured dual-probe temperature difference from the trunk sap flow sensor, the sapwood flux density (F_d; g cm^{-2} s^{-1}) was calculated using Granier's (1987) empirical equations (2) as follows:

$$F_d = \alpha K^{\beta} \quad (2)$$

where α and β are fitting parameters determined by the calibration curve and estimated at 0.013 and 1.024, respectively (Song et al., 2023). K is the dimensionless fluid flow index, which is calculated using the following equation:

$$K = \frac{(\Delta Tmax - \Delta T)}{\Delta T} \quad (3)$$

where ΔT is the temperature difference (°C) between two probes at any given time and ΔTmax is the maximum value of ΔT (°C). The average sap flow density (J_s; g m^{-2} s^{-1}) in the tree's sapwood was calculated using the following equation:

$$J_s = \frac{\sum_{i=1}^{5} F_{di} \times A_{si}}{\sum_{i=1}^{5} A_{si}} \quad (4)$$

where i is the i^{th} sample tree, and F_{di} and A_{si} represent the sapwood sap flow density and sapwood area of the i^{th} sample tree, respectively. The canopy transpiration rate (T_{day}; mm s^{-1}) was calculated using :

$$T_{day} = J_s \times \frac{A_{st}}{A_g} \quad (5)$$

where A_{st} and A_g are the total sapwood area of trees in the plot (m^2), and J_s is defined

https://doi.org/10.5194/egusphere-2026-3094
Preprint. Discussion started: 23 June 2026

as in Eq. 4.

This study also collected observational data on the transpiration (T) during the growing season in the study area's PT plantations. A total of 48 T values were measured, covering nine meteorological stations, using two methods: (1) stem sap flow was measured using the heat probe method and converted to Tr_a; and (2) T was calculated using the water balance equation based on growing season precipitation (Pr, mm), runoff (R, mm), soil evaporation (E, mm), and the change in soil water storage (ΔS, mm) during the growing season: T = Pr-R-E +ΔS.

Soil moisture sensors (EC-5, Decagon, USA) connected to a CR1000 datalogger were used to monitor the SWC at 20, 40, 60, 80, 100, 160, 200, 300, and 500 cm below the soil surface. The sensors exhibited a measurement accuracy of ±3%. To calibrate the sensors, SWC was also measured monthly using an oven-drying method. The established calibration equations are shown in Table 1.

Table 1 Calibration equations for EC-5 soil moisture sensors in the *Pinus tabuliformis* L. plantations at the Ansai site.

Soil depth（cm）	calibration equation	R^2
0-20	y=0.5693x+1.7374	0.93
20-40	y=0.7054x+2.3079	0.91
40-60	y=0.7236x+3.2223	0.99
60-80	y=0.9646x+2.8214	0.93
80-100	y=1.0065x+5.7863	0.95
100-140	y=1.4498x+2.2259	0.93
140-160	y=1.5845x-0.0117	0.92
160-200	y=1.0123x+4.7166	0.88
200-300	y=0.664x+3.2464	0.93
300-500	y=0.5928x+2.7618	0.87

https://doi.org/10.5194/egusphere-2026-3094
Preprint. Discussion started: 23 June 2026

Ψ_{md} was measured between 12:00 PM and 2:00 PM each month during the growing season using a portable plant water potential meter (PMS Instrument Co., Corvallis, OR, USA). For each measurement, a branch exposed to sunlight was cut from the upper-middle canopy using pruning shears. Pine needle samples were collected from the harvested branch using a small knife, and a bundle of pine needles immediately wrapped tightly with raw tape. Samples were then put in the pressure chamber for measurement. Simultaneously, an electronic magnifying glass was used to observe the condition of the petiole cut surface. When small water droplets appeared on the petiole cut surface, the inflation valve was quickly closed and the numbers on the pressure gauge interface recorded, which represented the instantaneous Ψ_{md}. Each treatment included six replicates.

2.3.2 Growth process validation

To evaluate the growth process of the BBGC-Sperry model, this study collected observational data on aboveground biomass (AGB) during the growing season in the study area's PT plantations. AGB is highly correlated with indicators such as NPP and LAI. Therefore, AGB can be considered a representative indicator that is readily available. A total of 74 AGB values were obtained using the allometric growth equation (Table 2), covering 27 meteorological stations.

Table 2 Biomass equations for *Pinus tabuliformis* L. (Zhou et al., 2018)

Organs	Biomass equations	R^2
Stems	$W=0.0485\times(D^2H)^{0.8510}$	0.99
Branches	$W=0.0245\times(D^2H)^{0.7991}$	0.99
Leaves	$W=0.0500\times(D^2H)^{0.6308}$	0.98

https://doi.org/10.5194/egusphere-2026-3094
Preprint. Discussion started: 23 June 2026

Roots	$W=0.0298\times(D^2H)^{0.7866}$	0.99

Notes: W represents biomass (kg C m^{-2}); D is diameter at breast height (cm); H is tree height (m).

2.4 Data sources

2.4.1 Meteorological datasets

Meteorological data for 130 simulated sites from 2000 to 2024 were obtained from the China National Meteorological Center (http://data.cma.cn/), including daily maximum temperature, minimum temperature, relative humidity, and precipitation, among other meteorological data. Future meteorological data were obtained from NASA's Earth Exchange Global Daily Downscaled Projections (NEX-GDDP-CMIP6) (https://doi.org/10.7917/OFSG3345) (Thrasher et al., 2022). This dataset features a resolution of 0.25°. We selected daily datasets for six models (CanESM5, FGOALS-g3, GFDL-CM4, IPSL-CM6A-LR, MPI-ESM1-2-HR, and MRI-ESM2-0) under three scenarios (SSP126, SSP245, and SSP585). The CO_2 emissions under the three scenarios are shown in Fig. S1 (Melnikova et al., 2023). The datasets include daily maximum temperatures, daily minimum temperatures, and precipitation data for the period 2025–2099 for the same 130 meteorological stations.

Based on the phased characteristics of carbon dioxide emission trajectories under different Shared Socioeconomic Pathways (SSP) scenarios, and considering the period around 2050 marks a critical turning point for multiple emission scenarios, both SSP126 and SSP245 exhibit a trend of flat or slowly declining emissions after 2075. To more accurately depict dynamic changes in various variables, this study divided the future

https://doi.org/10.5194/egusphere-2026-3094
Preprint. Discussion started: 23 June 2026

time period into three phases: near-future period (NFP; 2025-2049), mid-future period (MFP; 2050-2074), and far-future period (FFP; 2075-2099). The Mountain Climate Simulator (MT–CLIM) program (https://www.umt.edu/numerical-terradynamic-simulation-group/project/mt-clim.php) (Thornton et al., 2002) was used to calculate solar radiation, daylight average partial pressure of water vapor, and day length based on acquired meteorological data.

2.4.2 Soil hydraulic properties

The soil parameters required for this study included saturated soil moisture content (θ_s), residual soil moisture content (θ_r), soil parameters (α and n), and saturated hydraulic conductivity (K_s). At the Ansai experimental site, we measured K_s and soil moisture characteristic curves using the ring knife method in the laboratory. We derived the VG model using RETC software to determine other soil hydraulic parameters (van Genuchten, 1980). Clay, silt, sand, and bulk density data for the 130 simulated sites were obtained from the SoilGrid250m dataset (https://www.soilgrids.org/). Soil K_s was sourced from the Northwest Arid Region Soil Hydraulic Parameters dataset (Zhang et al., 2024a). Soil moisture characteristic curves were obtained using the Arya-Paris model (Arya et al., 1999), and the VG model was also derived using RETC software to determine θ_s, θ_r, α, and n.

2.4.3 Eco-physiological parameters

The ecological and physiological parameters and values used in this simulation are shown in Table S1, along with those for PT plantations in the Biome-BGC model from previous studies. Xylem vulnerability curves (VCs) for PT were determined using the

https://doi.org/10.5194/egusphere-2026-3094
Preprint. Discussion started: 23 June 2026

benchtop dehydration method (Sperry et al., 1988) (Fig. S2). We assumed VC parameters were the same for roots, stems, and leaves. The maximum whole-plant hydraulic conductance per leaf area, maximum diffusive conductance, and average proportion of rhizosphere resistance were determined based on transpiration rates observed at the Ansai site in 2024 (Sperry et al., 2016; Tai et al., 2018; Wolfe et al., 2016).

2.5 Assessment of drought-induced mortality risk

Under drought stress, plants regulate stomatal function to influence carbon metabolism processes, which is considered a core mechanism in drought-induced mortality. A prolonged high daily percentage loss of whole-plant hydraulic conductance (PLK) serves as a key indicator of drought mortality risk, calculated as follows:

$$PLK=\left(1-\frac{k_{plant}}{k_{max}}\right)\times 100\% \quad (6)$$

where k_{plant} is the whole plant hydraulic conductance and k_{max} is the maximum soil-plant hydraulic conductance. Annual average PLK (APLK, %) reflects an inter-annual variation in plant hydraulic security. We assumed the xylem embolism of PT could not be recovered during the growing season. New plant tissue growth the next spring results from the generation of root and stem pressure (Choat et al., 2018). An APLK value of 60% is widely accepted to represent the threshold at which trees face a high risk of mortality (McDowell et al., 2013). Therefore, we also used this value to assess the drought-induced mortality risk. Furthermore, we defined the probability value where APLK ≥ 60% as DMRP. The primary long-term objectives for the PT plantations in this study area are soil and water conservation and ecosystem restoration. The functional

https://doi.org/10.5194/egusphere-2026-3094
Preprint. Discussion started: 23 June 2026

cycle for stand stability of PT plantations ranges from 20 to 50 years (Zhang et al., 2024b). The study area is divided into high-risk (DMRP > 5%), medium-risk (2% ≤ DMRP ≤ 5%), and low-risk (DMRP < 2%) zones with drought mortality event recurrence intervals of < 20, 20-50, and > 50 years, respectively.

2.6 Calculation of carbon-water-hydraulic risk index

To comprehensively assess the impact of future climate change on the sustainability of PT plantations, this study developed a carbon-water-hydraulic risk index (CWHRI) by integrating carbon assimilation, water consumption, and plant hydraulic risk into a unified metric. These three components were selected because they represent key dimensions of plantation functioning that are commonly evaluated separately. Specifically, NPP reflects carbon sequestration and serves as the positive contribution to sustainability, ET characterizes water consumption, and DMRP represents the probability of tree mortality associated with drought-induced hydraulic stress. The CWHRI is formulated as follows:

$$\mathrm{CWHRI} = \frac{\mathrm{NPP}}{\mathrm{ET}} \times (1 - \mathrm{DMRP}) \tag{7}$$

where (1-DMRP) represents the survival probability under drought stress. The unit of CWHRI is g C kg^{-1} H_2O, representing the expected carbon gain per unit water consumed after accounting for drought-induced mortality risk. The multiplicative form ensures that as DMRP approaches 1 (certain mortality), CWHRI approaches zero regardless of NPP or ET, reflecting the reality that a dying tree contributes nothing to ecosystem function even if its short-term productivity appears normal. A higher value of CWHRI indicates safer water transport in plantations and greater efficiency in using

https://doi.org/10.5194/egusphere-2026-3094
Preprint. Discussion started: 23 June 2026

water to support growth.

2.7 Statistical analyses

Annual mean NPP, ET,, APLK, DMRP, and CWHRI were calculated for the baseline period and NFP, MFP, and FFP under three future climate scenarios (SSP126, SSP245, and SSP585). Spatial distribution maps were generated using Kriging interpolation in ArcGIS 10.8 software. Annual values for the study area were obtained by weighting annual data from 130 stations using the Thiessen polygons method. Temporal variations of indicators were analyzed using one-way analysis of variance (ANOVA), with multiple comparisons performed using Duncan's test at a significance level of $p<0.05$. A multiple linear regression method was used to calculate the contribution of NPP, ET, and DMRP to changes in CWHRI. The importance of six meteorological variables (mean annual precipitation, MAP; mean annual temperature, MAT; mean annual maximum temperature, MAT_{max}; mean annual minimum temperature, MAT_{min}; mean annual vapor pressure deficit, VPD, mean annual soil water storage, SWS**)** to dynamic changes of CWHRI was assessed using XGBoost. Hyperparameters were tuned through five-fold cross-validation combined with grid search, while early stopping was applied to track validation error (Gong et al., 2026). The key variables identified by the XGBoost model were considered as the driving factors behind dynamic changes in CWHRI.

Model accuracy was evaluated using the coefficient of determination (R^2), mean absolute error (MAE), root mean square error (RMSE), relative root mean square error (rRMSE), and Nash-Sutcliffe efficiency coefficient (NSE) (Zhang et al., 2024b). The

https://doi.org/10.5194/egusphere-2026-3094
Preprint. Discussion started: 23 June 2026

NSE is used to measure the goodness of fit of a model, with values closer to 1.0 indicating higher simulation accuracy. Lower values of MAE, RMSE, and rRMSE indicate higher accuracy.

3 Results

3.1 BBGC-Sperry model evaluation

Validation of the BBGC-Sperry model included hydraulic and growth processes. Specifically, hydraulic process validation data were based on T_{day}, SWC in the 0-500 cm profile, and Ψ_{md} at the Ansai site during the 2024 and 2025 growing seasons (May 1 to September 30), as well as multi-point transpiration data during the growing season. As shown in Fig. 2a-g, the R^2 coefficient between the simulated and observed T_{day} was 0.87, with NSE, MAE, RMSE, and rRMSE values of 0.80, 0.22 mm d^{-1}, 0.31 mm d^{-1}, and 21.83%, respectively. For SWC (0-500 cm), the R^2 value between the simulated and observed values was 0.96, with NSE, MAE, RMSE, and rRMSE values of 0.99, 0.00 cm^3 cm^{-3}, 0.00 cm^3 cm^{-3}, and 1.69%, respectively. The R^2 value for Ψ_{md} between the simulated and observed values was 0.98, with NSE, MAE, RMSE, and rRMSE of 0.99, 0.05 MPa, 0.06 MPa, and -4.00%, respectively. The R^2 between the simulated and observed T was 0.86, with NSE, MAE, RMSE, and rRMSE values of 0.85, 22.60 mm, 31.04 mm, and 13.55%, respectively. These results indicate the BBGC-Sperry model can effectively simulate dynamic changes in hydraulic processes during the growing season of PT plantations on the Loess Plateau.

Growth process validation data were based on AGB observations from 36 sites in

https://doi.org/10.5194/egusphere-2026-3094
Preprint. Discussion started: 23 June 2026

the study area. The R^2 value between the simulated and observed AGB was 0.81, with NSE, MAE, RMSE, and rRMSE values of 0.80, 0.42 kg C m^{-2}, 0.93 kg C m^{-2}, and 44.61%, respectively (Fig. 2h). These results indicate the BBGC-Sperry model can accurately simulate water transport and growth processes for PT plantations at both spatial and temporal scales. The high correlation between T, ET, AGB, and NPP indicates the BBGC-Sperry model can also effectively simulate long-term dynamic changes in NPP and ET in this region.

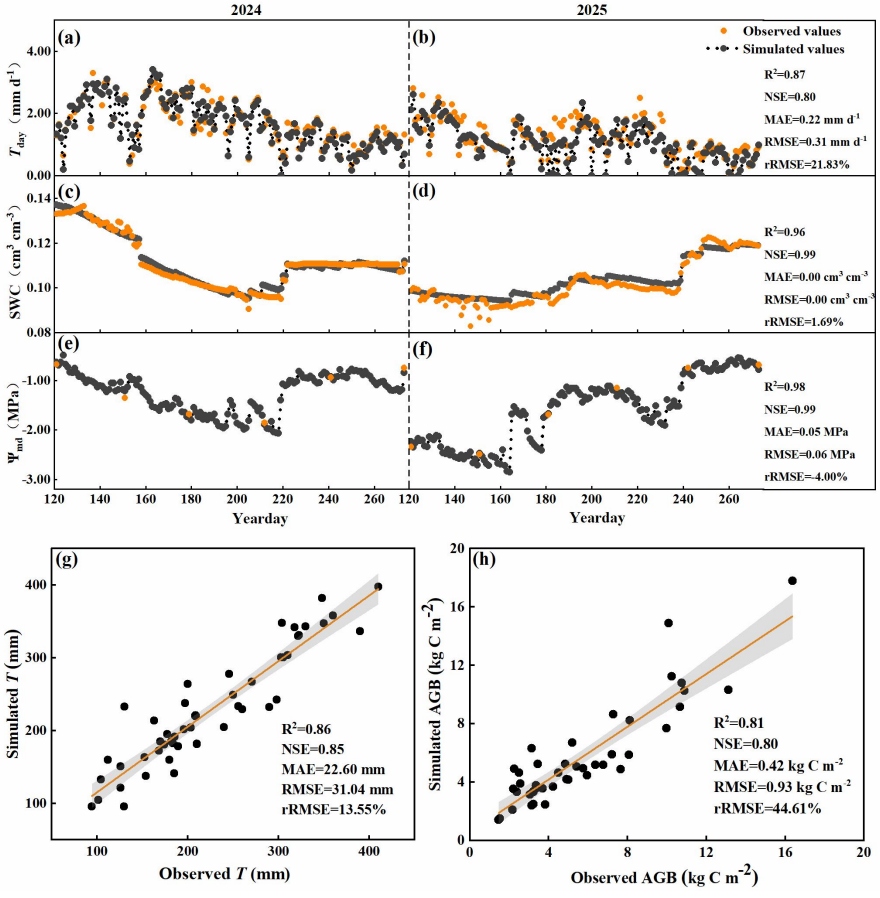

Figure. 2 Comparison of simulated and observed values for artificial *Pinus tabuliformis* L. plantations during the growing seasons of 2024 and 2025: (a)-(b) daily transpiration

https://doi.org/10.5194/egusphere-2026-3094
Preprint. Discussion started: 23 June 2026

(T_{day}), (c)-(d) average soil water content (SWC) in the 0–500 cm soil profile, (e)-(f) midday leaf water potential (Ψ_{md}), (g) multi-point transpiration during the growing season (T), and (h) aboveground biomass (AGB).

3.2 Projected climate change

We validated the simulation performance of the regional climate models by comparing observed climate data for the historical period (1979-2014) with the simulation results from a single climate model and a multi-model average (Fig. 3). The multi-model average demonstrated the best performance. Specifically, the correlation coefficient between observed and simulated monthly precipitation ranged from 0.5 to 0.7 (Fig. 3), while the correlation coefficients for monthly minimum and maximum temperatures exceeded 0.9 (Fig. 3b, c). These results indicate these downscaled data effectively represent the actual climate conditions of the study area. Therefore, multi-model average climate data were employed to simulate the response of PT plantations to future climate change.

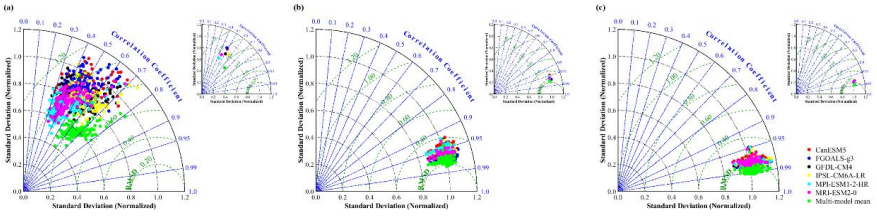

Figure. 3 Taylor diagrams of monthly precipitation (a), monthly maximum temperature (b), and monthly minimum temperature (c) at 130 meteorological stations in the study area from 1979 to 2014. The upper-right plot represents the mean values across all

https://doi.org/10.5194/egusphere-2026-3094
Preprint. Discussion started: 23 June 2026

453 stations. Each color corresponds to a climate model or multi-model ensemble. The
454 green dashed line represents the root mean square error (RMSE).
455
456 Based on the linear trends (slope values) of MAP, MAT, MAT_{max}, and MAT_{min} from
457 2000 to 2099, we analyzed the spatiotemporal changes in climate during the study
458 period (Fig. 4). The slope values of climate variables under different SSPs showed
459 significant spatial heterogeneity (Fig. 4a-l). The highest slope values were mainly
460 concentrated in the southeastern part of the study area, with a general decrease from
461 southeast to northwest. Under the SSP126 scenario, 52.9% of the region showed an
462 increasing trend in MAP during the study period, primarily in the southwest and
463 southeast, with 32.8% of the area experiencing significant increases ($p<0.05$).
464 Conversely, decreases in MAP were mainly located in the central and northern regions.
465 MAT exhibited an increasing trend over a larger portion of the study area, covering
466 71.5%, with 58.9% of the area experiencing significant increases ($p<0.05$). Decreases
467 in MAT were limited to the southwest and northeast regions. MAT_{max} primarily
468 increased in the central region, while decreasing regions were limited to the southwest
469 and northeast. MAT_{min} primarily increased in the western and central regions, while
470 decreasing regions were limited to the northeast and southeast. Compared to the
471 SSP126 scenario, over 95% of the study area showed increases in MAP and MAT under
472 the SSP245 and SSP585 scenarios. The areas with the largest increases were
473 concentrated in the southern part of the study area.
474 Fig. 4m-o shows future climate in the study area is expected to be warmer and

https://doi.org/10.5194/egusphere-2026-3094
Preprint. Discussion started: 23 June 2026

wetter overall compared to the baseline period. Under the SSP126 scenario, MAP ranged from 482 to 633 mm, with an average increase of -0.105 mm y^{-1}. In contrast, MAT ranged from 12.99 to 14.64 ℃, with an average increase of 0.020 ℃ y^{-1}. MAT_{max} ranged from 15.79 to 17.97 ℃, with an average increase of 0.025 ℃ y^{-1}. MAT_{min} values ranged from 5.21 to 6.46 ℃, with an average increase of 0.007 ℃ y^{-1}. Under the SSP245 scenario, MAP values ranged from 524 to 769 mm, with an average increase of 0.77 mm y^{-1}. Notably, the MAP growth rate fluctuated. In contrast, MAT increased more steadily, with an average increase of 0.014 ℃ y^{-1} for MAT, 0.010 ℃ y^{-1} for MAT_{max}, and 0.025 ℃ y^{-1} for MAT_{min}. Under the SSP585 scenario, the average increases of MAP, MAT, MAT_{max}, and MAT_{min} were 1.806 mm y^{-1}, 0.070 ℃ y^{-1}, 0.069 ℃ y^{-1}, and 0.060℃ y^{-1}, respectively. Overall, the FFP climate is expected to experience the most significant fluctuations under the SSP585 scenario ($p<0.05$).

https://doi.org/10.5194/egusphere-2026-3094
Preprint. Discussion started: 23 June 2026

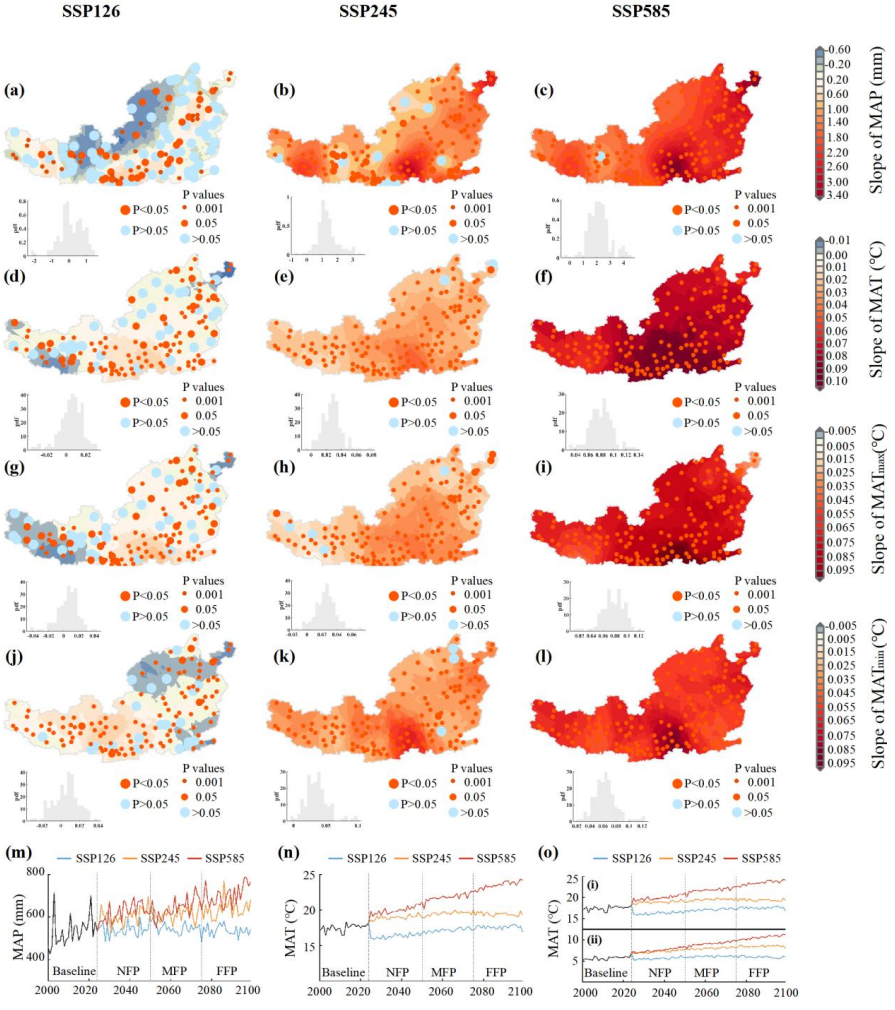

Figure. 4 Spatiotemporal dynamics in mean annual precipitation (MAP), mean annual temperature (MAT), mean annual maximum temperature (MAT_{max}), and mean annual minimum temperature (MAT_{min}) within the study area from 2000 to 2099 under SSP126, SSP245, and SSP585 scenarios: (a)-(l), spatial distributions of linear trend slopes for each variable under the three scenarios, with probability density functions (PDFs) shown in the lower-left corner; (m)-(o), temporal variation of MAP, MAT, MAT_{max}(i), and MAT_{min} (ii) under all SSP scenarios.

https://doi.org/10.5194/egusphere-2026-3094
Preprint. Discussion started: 23 June 2026

3.3 Spatiotemporal dynamics of NPP and ET

Fig. 5 shows spatiotemporal changes in the mean annual NPP of PT plantations during the baseline and future periods. The NPP of the study area was 533.5 g C m^{-2} yr^{-1} in the baseline period but significantly lower in the future periods under the SSP126 and SSP245 scenarios (Fig. 5a, b). However, the NPP in the FFP was 577.9 g C m^{-2} yr^{-1} under the SSP585 scenario, which is significantly higher than in the baseline period (Fig. 5c). The highest NPP values of the baseline period were in the south and central regions, and the lowest were in the west, with a gradual decrease noted from southeast to northwest. This distribution pattern continues in the future periods.

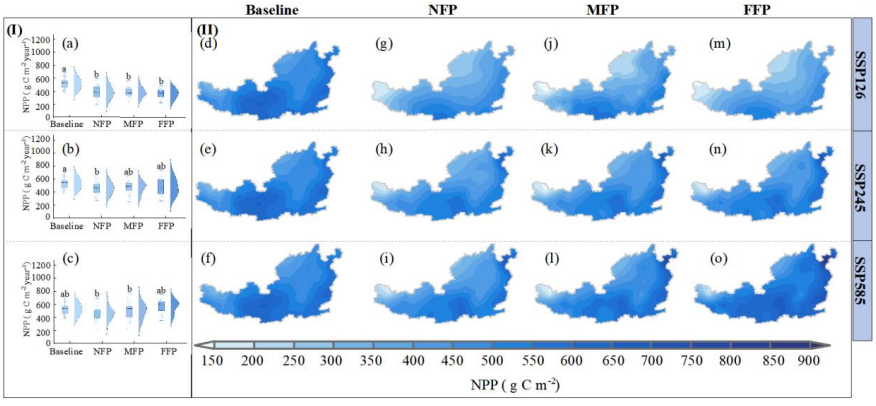

Figure. 5 Projected spatiotemporal dynamics of net primary production (NPP) for *Pinus tabuliformis* L. in the study area under baseline, SSP126, SSP245, and SSP585 scenarios: (I) temporal changes in NPP, with different letters indicating significant differences among the four periods within each scenario ($p<0.05$); (II) spatial dynamics of NPP. Baseline refers to the reference period (2000-2024), NFP to the near-future

https://doi.org/10.5194/egusphere-2026-3094
Preprint. Discussion started: 23 June 2026

period (2025-2049), MFP to the mid-future period (2050-2074), and FFP to the far-future period (2075-2099).

Fig. 6 shows the spatiotemporal changes in the mean annual ET values during the baseline and future periods. The ET was 572.9 mm during the baseline period and showed no significant changes under the SSP126 scenario in the future periods. However, it significantly increased under the SSP245 scenario and particularly under the SSP585 scenario (Fig. 6c). The ET value decreased gradually from southeast to northwest in the baseline period. This pattern was maintained in all SSPs.

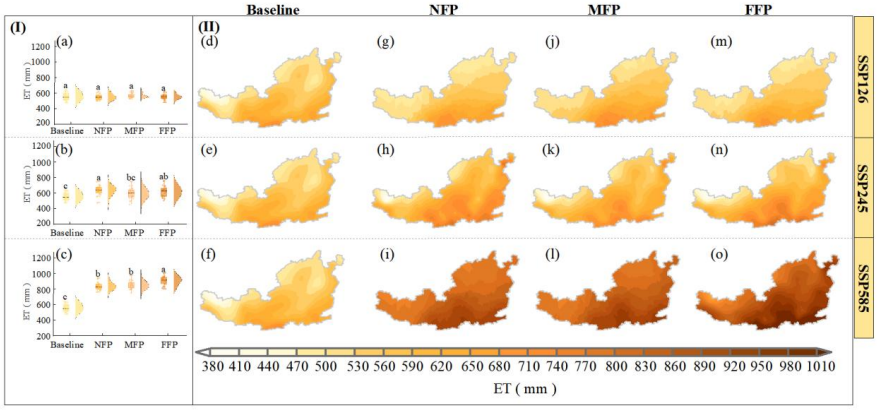

Figure. 6 Projected spatiotemporal dynamics of annual mean actual evapotranspiration (ET) for *Pinus tabuliformis* L. in the study area under baseline, SSP126, SSP245, and SSP585 scenarios: (I) temporal changes of ET, with different letters indicating significant differences among the four periods within each scenario ($p<0.05$); (II) spatial dynamics of NPP. Baseline, NFP, MFP, and FFP are the same as defined in Fig. 5.

https://doi.org/10.5194/egusphere-2026-3094
Preprint. Discussion started: 23 June 2026

3.4 Spatiotemporal dynamics of APLK and DMRP

Fig. 7 shows spatial and temporal changes in the annual APLK of PT plantations in the study area during the baseline and future periods. APLK for the baseline period was 24.9%. Under the SSP126 scenario, APLK values in the NFP, MFP, and FFP were 28.2, 28.7, and 29.5%, respectively, indicating an increasing trend with a relatively slow rate of change. Under the SSP245 scenario, APLK values for future periods were 29.1% (NFP), 33.3% (MFP), and 32.8% (FFP), indicating a larger increase compared to the baseline period. Under the SSP585 scenario, APLK values increased the most, with NFP, MFP, and FFP values of 31.7%, 41.1%, and 46.4%, respectively, indicating APLK values will significantly increase under a more severe climate change context. APLK values during the baseline period showed an increasing trend from southeast to northwest. In the future, high APLK values will gradually expand from the northwest and northeast to the central and southern regions. Under the SSP585 scenario, only very central and southern regions have APLK values below 35%, while most areas in the central and northern regions have values above 50% in the FFP (Fig. 7o).

https://doi.org/10.5194/egusphere-2026-3094
Preprint. Discussion started: 23 June 2026

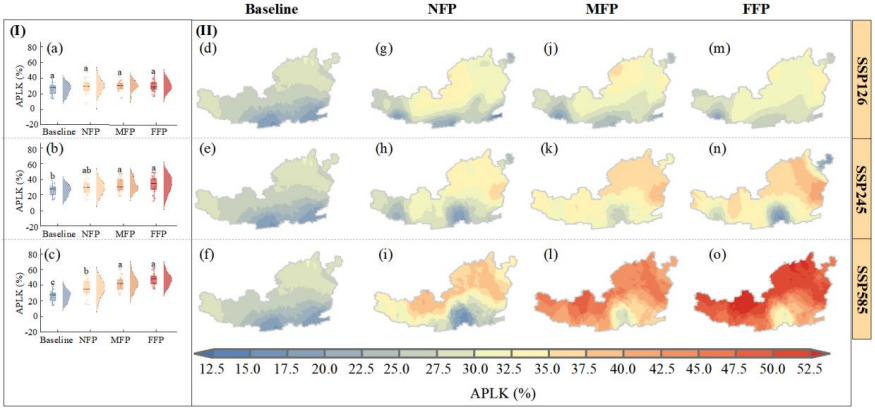

Figure. 7 Projected spatiotemporal dynamics of annual average percentage loss of whole-plant hydraulic conductance (APLK) for *Pinus tabuliformis* L. in the study area under baseline, SSP126, SSP245, and SSP585 scenarios: (I) temporal changes of APLK, with different letters indicating significant differences among the four periods within each scenario ($p<0.05$); (II) spatial dynamics of NPP. Baseline, NFP, MFP, and FFP are the same as defined in Fig. 5.

Based on a threshold of APLK ≥ 60%, we calculated the spatiotemporal variations of DMRP of PT plantations during the baseline and future periods (Fig. 8). Low-risk zones for DMRP were mainly located in the southern part of the study area, medium-risk zones in the central and eastern regions, and high-risk zones in the northwest, north, and east, exhibiting a clear gradient from southeast to northwest in the baseline period. Under the SSP126 scenario, the distribution of high-risk zones will be similar to the baseline period, but the distribution of low- and medium-risk zones will change. In the NFP, low-risk zones will be primarily concentrated in the west. In the MFP, low-risk zones will be primarily concentrated in the west, central, and eastern regions. In the

https://doi.org/10.5194/egusphere-2026-3094
Preprint. Discussion started: 23 June 2026

564 FFP, low-risk zones will be primarily concentrated in the central and eastern regions.
565 Under the SSP245 and SSP585 scenarios, the distribution patterns of low-, medium-
566 and high-risk zones will be similar to the baseline period but the high-risk zones will
567 generally expand from northwest to southeast, covering a larger area. DMRP shows an
568 increasing trend under the SSP245 and SSP585 scenarios, but a slight decreasing trend
569 under the SSP126 scenario.

570

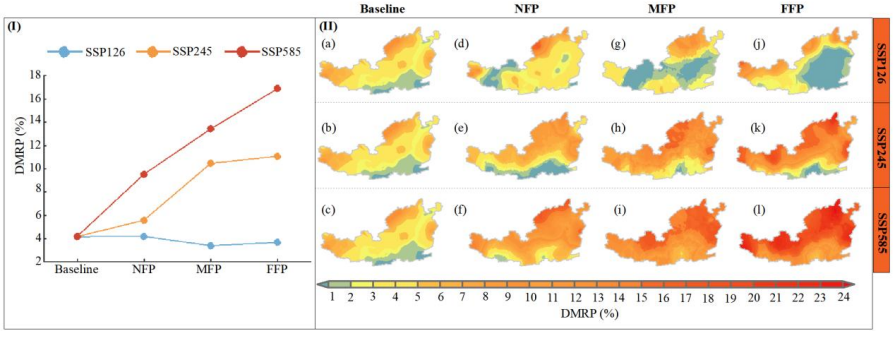

571

572 **Figure. 8** Projected spatiotemporal dynamics of drought-induced mortality risk
573 probability (DMRP) for *Pinus tabuliformis* L. in the study area under baseline, SSP126,
574 SSP245, and SSP585 scenarios: (I) temporal changes of DMRP; (II) spatial dynamics
575 of DMRP. Baseline, NFP, MFP, and FFP are the same as defined in Fig. 5.

576

577 **3.5 Spatiotemporal dynamics and factors influencing CWHRI**

578 To comprehensively assess the growth of PT plantations, NPP, ET, and DMRP were
579 used to calculate the CWHRI (Fig. 9). The CWHRI during the baseline period was 0.89
580 g C kg^{-1} H_2O and will decrease under the SSP126, SSP245, and SSP585 scenarios to
581 0.63-0.67, 0.66-0.67, and 0.50-0.51 g C kg^{-1} H_2O, respectively. This indicates the

https://doi.org/10.5194/egusphere-2026-3094
Preprint. Discussion started: 23 June 2026

582 growth of PT plantations will be retarded in the future and more susceptible to hydraulic
583 failure and even death. CWHRI showed considerable spatial variability, with low-value
584 zones mainly located in the western and northern parts of the study area, showing a
585 distinct decreasing gradient from southeast to northwest in the baseline period. This
586 pattern was maintained in all SSPs. Generally, areas with low CWHRI values will
587 expand in the future periods. Under the SSP585 scenario, the CWHRI in the western
588 parts of the study area will even fall below 0.25 g C kg^{-1} H_2O. This suggests PT
589 plantations in the western and northern parts of the study area will find it even more
590 challenging to survive.
591

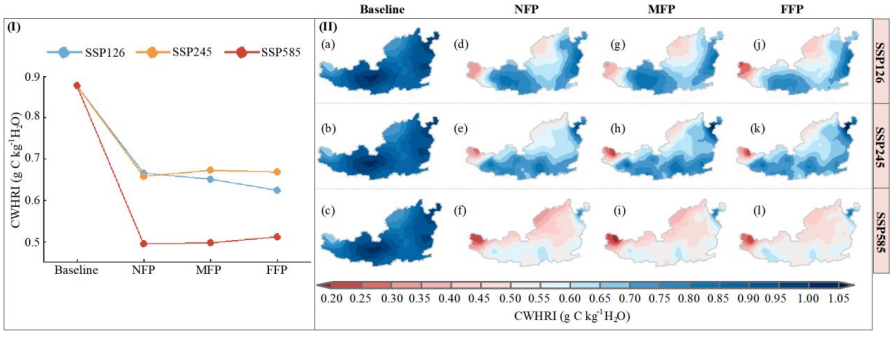

592

593 **Figure. 9** Projected spatiotemporal dynamics of the carbon-water-hydraulic risk index
594 (CWHRI) for *Pinus tabuliformis* L. in the study area under baseline, SSP126, SSP245,
595 and SSP585 scenarios: (I) temporal changes of CWHRI; (II) spatial dynamics of
596 CWHRI. Baseline, NFP, MFP, and FFP are the same as defined in Fig. 5.
597

598 To quantify the extent to which NPP, ET, and DMRP influence changes in the
599 CWHRI, we used multiple linear regression to calculate the relative contribution of

https://doi.org/10.5194/egusphere-2026-3094
Preprint. Discussion started: 23 June 2026

each variable (Fig. 10a). During the baseline period, net NPP and ET can explain 98% of the variation in CWHRI. NPP and ET remain the main factors affecting CWHRI in the future; however, the contribution of DMRP will continue to increase in all SSPs over the three future periods, reaching 17% in the FFP under the SSP585 scenario.

To deepen understanding of the factors driving CWHRI and how the relative importance of these factors changes, Fig. 10b presents an XGBoost-based assessment of the relative importance of six environmental factors for regions with different risk levels during the baseline and future periods. In the baseline period, VPD and SWS ranked as the top contributors. Specifically, the relative importance of VPD was 86% in the low-risk zones, and of SWS was 42% and 61% in the medium- and high-risk zones, respectively. Under the SSP126 scenario, VPD will remain the primary factor but its relative importance will decrease by 49% and 59% in the low-risk zones during the NFP and MFP, respectively. MAP will rank as the top contributor in the low-risk zones during the FFP, with a relative importance of 56%. In the medium-risk zones, MAP will be the primary factor during the NFP and MFP. SWS will be the main factor during the FFP, similar to the baseline period. In high-risk zones, MAP will be the main factor in all three periods, with relative importance ranging from 62% to 81%. Under the SSP245 scenario, MAT_{max} will be the main factor in the NFP and FFP in low-risk zones, with a relative importance of 51% and 60%, respectively. MAP,VPD and MAT_{max} will rank as the top contributors in the MFP, with the relative importance of these three factors being 91%. In the medium-risk zones, MAP will be the main factor in the NFP and MFP, while MAT_{max} will be the main factor in the FFP. In high-risk

https://doi.org/10.5194/egusphere-2026-3094
Preprint. Discussion started: 23 June 2026

zones, MAP will be the main factor in all three periods, with relative importance ranging from 67% to 76%. Under the SSP585 scenario, VPD will be the primary factor in low-risk zones during all three future periods, with a relative importance over 50%. In medium-risk zones, MAT_{max} will be the primary factor during the NFP and MFP, with a relative importance over 70%. VPD will be the primary factor during the FFP, with a relative importance of 99% highlighting the strong sensitivity of the CWHRI to atmospheric drought in the FFP. In high-risk zones, MAP will be the main factor in all three periods, with relative importance ranging from 49% to 68%. Generally, the relative importance of MAP and MAT_{max} will increase from the baseline period into the future, reflecting the moisture- and temperature-driven characteristics of the CWHRI under future climate change.

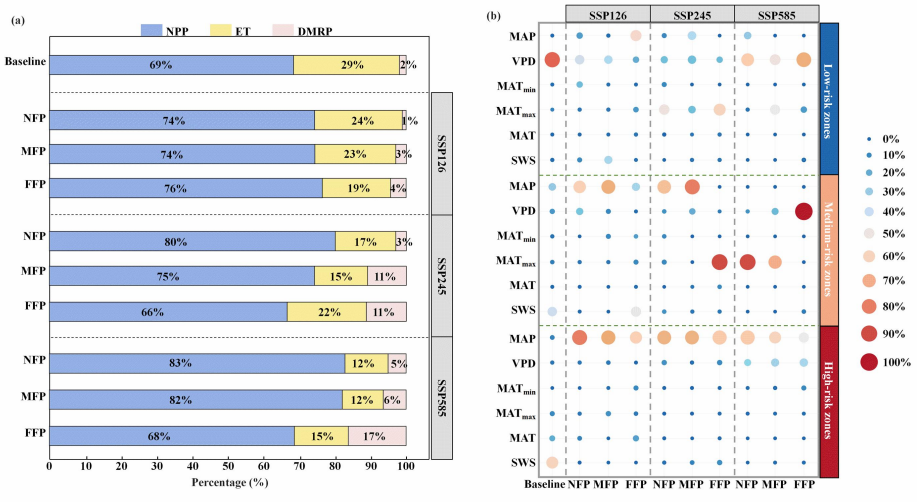

Figure. 10 Analysis of factors influencing variation in the carbon-water-hydraulic risk index (CWHRI): (a) contributions of net primary productivity (NPP), ecosystem

https://doi.org/10.5194/egusphere-2026-3094
Preprint. Discussion started: 23 June 2026

evapotranspiration (ET), and drought-induced mortality risk (DMRP) as determined by multiple linear regression analysis; (b) analysis of the relative importance of six environmental variables. MAP, mean annual precipitation; MAT mean annual temperature; MAT_{max}, mean annual maximum temperature; MAT_{min}, mean annual minimum temperature; VPD, mean annual vapor pressure deficit, SWS, mean annual soil water storage. Low-risk zones, DMRP < 2%. Medium-risk zones, 2% ≤ DMRP ≤ 5%. High-risk zones, DMRP > 5%.

4 Discussion

4.1 BBGC-Sperry Model performance

The BBGC-Sperry model is a coupled model. Therefore, a thorough validation is essential when using this model for simulation and prediction (Yan et al., 2022). Transpiration, SWC, Ψ_{md}, and AGB are critical indicators for assessing the complex effects of climate change on vegetation growth and physiological characteristics. Accordingly, we validated the reliability of the BBGC-Sperry model in simulating the growth dynamics of PT plantations by using data from 36 meteorological stations on the Loess Plateau (Fig. 2). The results indicate R^2 and NSE values for all simulated and measured indicators exceed 0.8, demonstrating the model effectively captures the dynamic changes in growth and ecohydrological processes in the PT plantations. This ability is closely tied to the model structure and input parameters.

The Sperry model replaces the SPAC water transport module of the original Biome-BGC model with an improved soil moisture transport module developed by Huang et

https://doi.org/10.5194/egusphere-2026-3094
Preprint. Discussion started: 23 June 2026

al. (2013). This allows for greater control over dynamic changes in plant hydraulic traits and enables the simulation of interactions among the water, carbon, and nitrogen cycles. The BBGC-Sperry model provides a more refined simulation of vegetation growth processes and physiological mechanisms than the original model, and has been successfully applied to the Loess Plateau (Zhang et al., 2020, 2024b; Yan et al., 2022). Meteorological parameters were sourced from continuous observational data, and soil and vegetation physiological parameters were derived from field measurements or published literature, thereby ensuring the accuracy of the validation process.

4.2 Changes of NPP, ET and DMRP for *Pinus tabuliformis* L. plantation

Against the backdrop of global warming, the study area is projected to become generally warmer and wetter in the future. Particularly under the SSP245 and SSP585 scenarios, average temperatures and precipitation will increase. These findings are consistent with previous studies (Xu et al., 2024). An assessment of the growth status of planted forests must not only consider their carbon sequestration capacity but also involve a comprehensive evaluation of related water fluxes and transport processes. Especially in water-scarce regions, water availability is the primary factor limiting the growth of planted forests. Considerable research shows that relying solely on indicators such as leaf area index, carbon sequestration, and ET to assess vegetation growth is insufficient as these superficial indicators may mask the physiological stress experienced by the vegetation (Tang et al., 2026).

Thus, we used the BBGC-Sperry model not only to simulate carbon and water fluxes of the PT plantations in the study area (Fig.s 5 and 6) but also to simulate

https://doi.org/10.5194/egusphere-2026-3094
Preprint. Discussion started: 23 June 2026

indicators that reflect vegetation physiology (Fig.s 7 and 8). The results show NPP in the study area will, in general, significantly decrease compared to the baseline period while the ET, APLK, and DMRP will significantly increase. Precipitation, temperature, and carbon dioxide concentrations all significantly impact NPP. Previous studies show increasing precipitation generally improves the water-use efficiency of vegetation and that moderate temperature increases and rising carbon dioxide concentrations promote photosynthesis. However, rising temperatures will decrease precipitation-use efficiency, thereby negatively impacting NPP (Gong et al., 2026). At the same time, high temperatures can inhibit the opening of plant stomata, thereby reducing plant productivity (He et al., 2024). Furthermore, NPP shows an upward trend across all three periods under all SSPs considered. This is primarily due to increased precipitation and carbon dioxide concentrations, which promote vegetation growth (Walker et al., 2021; Yan et al., 2022; Ouyang et al., 2014). ET is also projected to trend upward due to the combined effects of increased precipitation and rising temperatures. Precipitation serves as a source of water for ET. Rising temperatures prolong ET, thereby directly increasing atmospheric water demand and promoting the transfer of more water from the soil and vegetation into the air. Chai et al. (2025) and Lu et al. (2025) also reported this phenomenon.

These macroscopic observations reveal profound changes in plant hydraulic mechanisms. As climate change intensifies from the baseline period to the SSP126, SSP245, and SSP585 scenarios, rising temperatures combined with increased potential ET trigger mechanisms of plant hydraulic failure, as evidenced by significant increases

https://doi.org/10.5194/egusphere-2026-3094
Preprint. Discussion started: 23 June 2026

in APLK and DMRP. The intensification of hydraulic failure leads to a decline in stomatal conductance, which in turn impairs cell turgor, membrane permeability, and xylem conduction, significantly increasing plant vulnerability to heat stress and outbreaks of pests and diseases (Torres-Ruiz et al., 2024). This ultimately results in limited photosynthetic rates and a significant decline in productivity. The findings from this study are consistent with previous research. Bonal et al. (2016) pointed out that tree mortality caused by drought and high temperatures not only reduces regional NPP but also weakens the cooling effect of ET, thereby creating a positive feedback loop that exacerbates global warming. Choat et al. (2018) further found that even a slight increase in temperature may result in hydraulic imbalance or even death for most tree species. Notably, NPP, ET, and DMRP all show a synchronous increase in the FFP under the SSP585 scenario. This phenomenon may be attributed to the fact that, under extreme conditions, the offsetting effect of greater precipitation and CO_2 fertilization under SSP585, exceeding warming-induced productivity suppression. (Walker et al., 2021; Yan et al., 2022; Ouyang et al., 2014). Although we observe an increase in carbon accumulation, the internal physiological stress the plants endure also significantly increases. The above results indicate that relying solely on macroscopic indicators is insufficient to capture the true growth state of vegetation. Therefore, a comprehensive assessment method that incorporates water transport processes is of great significance for accurately predicting vegetation growth dynamics and stability under future climate change.

4.3 Changes of CWHRI for *Pinus tabuliformis* L. plantation

https://doi.org/10.5194/egusphere-2026-3094
Preprint. Discussion started: 23 June 2026

In this study, we further calculated the CWHRI based on the three fundamental indicators (NPP, ET, and DMRP) (Fig. 9). Compared to the baseline period, the CWHRI will significantly decline in the future, indicating PT plantation sustainability will face severe constraints. The greater fluctuations in NPP during the study period are the dominant factor affecting the CWHRI, but the relative importance of DMRP has been steadily increasing under all SSPs, rising from 2% during the baseline period to 17% in the FFP under SSP585. This increasing contribution indicates that although conventional water-use efficiency adequately characterizes carbon-water relationships under current and near-term conditions, failure to account for the increasing influence of hydraulic failure risk may lead to progressively optimistic estimates of long-term plantation sustainability. And this bias likely to accumulate over time. These findings also corroborate the concerns raised by Wang et al. (2025) regarding future vegetation growth.

The primary environmental factors influencing the CWHRI are related to the availability of water resources. During the baseline period, MAP, VPD, and SWS were the primary driving factors. In all SSPs, the importance of MAP and MAT_{max} increases, with these becoming the most significant drivers. SWS directly determines the amount of water available to vegetation, while MAT_{max} and VPD are related not only to the degree of environmental aridity but also the stomatal conductance of vegetation and upward water transport driven by transpiration (Wang et al., 2009; Wang et al., 2024; Tang et al., 2026). Therefore, these factors strongly influence the variability of CWHRI. These findings indicate water-related ecological factors and meteorological variables

https://doi.org/10.5194/egusphere-2026-3094
Preprint. Discussion started: 23 June 2026

remain key elements for future model improvements and ecological management strategies. Furthermore, the CWHRI declines steadily from the baseline period to the future periods, underscoring the urgency to formulate new management strategies and implement proactive intervention measures.

4.4 Limitations and implications

This study used the eco-hydrological BBGC-Sperry model to predict the growth, water consumption, and drought-induced mortality risk of PT plantations under future climate scenarios. The vegetation parameters in this model are fixed, which typically implies the spatiotemporal variability of vegetation growth is ignored, thereby introducing uncertainty into the simulation results. Recent studies based on the theory of plant hydraulic adaptation have predicted plant hydraulic, stomatal, and photosynthetic traits across various spatiotemporal scales (Joshi et al., 2022; Sperry et al., 2019). Future research should focus on integrating vegetation growth dynamics to further enhance model calibration and accuracy. We used meteorological data with a resolution of 0.25°, which effectively captures the dynamics of future climate change. However, limitations in accuracy may persist, particularly in precipitation prediction, which has notably lower accuracy. Spatially, we extended the simulated data from 130 meteorological stations across the region using Kriging interpolation. Although this method is computationally efficient, it may have limitations in resolution and accuracy. Additionally, although the BBGC-Sperry model has improved accuracy for simulating hydraulic transport processes compared to the original Biome-BGC model, the recently introduced BBGCMuSo model has more comprehensively simulated management

https://doi.org/10.5194/egusphere-2026-3094
Preprint. Discussion started: 23 June 2026

practices. These improvements need to be integrated into the BBGC-Sperry model to better analyze the ability of different management strategies to improve the sustainability of forest plantations.

Despite certain methodological limitations, this study provides valuable scientific insights for the sustainable development of PT plantations. Compared to previous simulations, our study offers a comprehensive explanation of the drought response mechanisms of PT plantations under future climate change. Notably, under the backdrop of global climate change, the CWHRI of plantations is projected decline and the contribution of DMRP has been steadily increasing under all SSPs, which indicated that current forest management practices may render years of restoration efforts ineffective.We recommend accurately assessing the optimal vegetation cover using soil moisture carrying capacity thresholds or early-warning models, implementing thinning management for existing PT plantations, as well as mixed-species planting in low-risk southeastern regions, slope engineering practices in moderate-risk central and western regions (Yang et al., 2023), and gradually converting plantations to drought-tolerant shrubs or sparse grasslands in high-risk northwestern regions, to increase plantation sustainability and enable proactive responses to future global climate change.

5 Conclusion

This study used the BBGC-Sperry model to simulate the spatiotemporal dynamics of PT plantations from 2000 to 2099 under future climate scenarios (SSP126, SSP245, SSP585) on the Loess Plateau. The key findings are as follows:

https://doi.org/10.5194/egusphere-2026-3094
Preprint. Discussion started: 23 June 2026

(1) The BBGC-Sperry model, verified using hydraulic and growth process data, can effectively simulate the growth of PT plantations and their drought-induced mortality risk probability.

(2) The growth of PT plantations will slow down in the future. During the 100-year period, NPP values of PT plantations are projected to significantly decline, except in the FFP under the SSP585 scenario. Overall, spatial change patterns reveal a gradual decline in vegetation growth from the southeast to northwest. ET is projected to show the opposite trend.

(3) The mortality risk for PT plantations will increase, and the affected area will also expand. The APLK and DMRP of PT plantations are projected to significantly increase in the future. The study area will gradually shift from low-to-medium risk areas in the southeast to medium-to-high risk areas in the northwest.

(4) Compared to the baseline period, the CWHSI of PT plantations is projected to significantly decline in the future. The contribution of DMRP to CWHRI variability rises steadily across all SSPs, indicating that hydraulic risk constitutes a key constraint on plantation sustainability under future climate change.

These findings provide a better understanding of the growth of PT plantations in the restoration areas and how they will respond to future climate change. These results suggest that assessments neglecting plant hydraulic risk may overestimate future plantation persistence, and highlight the importance of prioritizing hydraulic safety and tree survival in future plantation management.

https://doi.org/10.5194/egusphere-2026-3094
Preprint. Discussion started: 23 June 2026

Data availability

Data will be made available on request.

Author contributions

Tianqi Guo: Writing – original draft, Software, Methodology, Formal analysis, Data curation, Conceptualization.

Mingbin Huang: Writing – review & editing, Supervision, Project administration, Methodology, Funding acquisition, Conceptualization.

Zhongdian Zhang: Writing – review & editing.

Rui Liu: Writing – review & editing, Data curation.

Xiaofei Wu: Data curation.

Xinmei Liu: Writing – review.

Chenyi Ju: Writing – review.

Competing interests

The authors declare that they have no known competing financial interests or personal relationships that could have appeared to influence the work reported in this paper.

Acknowledgements

https://doi.org/10.5194/egusphere-2026-3094
Preprint. Discussion started: 23 June 2026

The authors thank the members of the Ansai Agricultural Ecology Station, Chinese Academy of Sciences for their assistance.

Financial support

This research was financially supported by the National Natural Science Foundation of China (No. 42177287).

References

Arend, M., Link, R. M., Patthey, R., Hoch, G., Schuldt, B., and Kahmen, A.: Rapid hydraulic collapse as cause of drought-induced mortality in conifers, Proc. Natl. Acad. Sci., 118, e2025251118, https://doi.org/10.1073/pnas.2025251118, 2021.

Arya, L. M., Leij, F. J., van Genuchten, M. T., and Shouse, P. J.: Scaling parameter to predict the soil water characteristic from particle-size distribution data, Soil Sci. Soc. Am. J., 63, 510 – 519, https://doi.org/10.2136/sssaj1999.03615995006300030013x, 1999.

Bonal, D., Burban, B., Stahl, C., Wagner, F., and Hérault, B.: The response of tropical rainforests to drought—lessons from recent research and future prospects, Ann. For. Sci., 73, 27 – 44, https://doi.org/10.1007/s13595-015-0522-5, 2016.

Brodribb, T. J., Powers, J., Cochard, H., and Choat, B.: Hanging by a thread? Forests and drought, Science, 368, 261 – 266, https://doi.org/10.1126/science.aat7631, 2020.

https://doi.org/10.5194/egusphere-2026-3094
Preprint. Discussion started: 23 June 2026

852 Chai, Y. F., Miao, C. Y., Slater, L., Ciais, P., Berghuijs, W. R., Chen, T. X., and
853 Huntingford, C.: Underestimating global land greening: Future vegetation changes
854 and their impacts on terrestrial water loss, One Earth, 8, 101176,
855 https://doi.org/10.1016/j.oneear.2025.101176, 2025.
856 Chen, C., Bongers, F. J., Schmid, B., Ma, K., and Liu, X. J.: Ecosystem consequences
857 of functional diversity in forests and implications for restoration, New Phytol., 247,
858 1081 – 1097, https://doi.org/10.1111/nph.70247, 2025.
859 Chen, H., Shao, M., and Li, Y.: Soil desiccation in the Loess Plateau of China,
860 Geoderma, 143, 91 – 100, https://doi.org/10.1016/j.geoderma.2007.10.013, 2008.
861 Chen, S. N., Wei, W., and Huang, Y.: Biophysical controls on canopy transpiration of
862 Pinus tabulaeformis under different soil moisture conditions in the Loess Plateau
863 of China, J. Hydrol., 631, 130799, https://doi.org/10.1016/j.jhydrol.2024.130799,
864 2024.
865 Chen, Z., Wang, W., Forzieri, G., and Cescatti, A.: Transition from positive to negative
866 indirect CO_2 effects on the vegetation carbon uptake, Nat. Commun., 15, 1500,
867 https://doi.org/10.1038/s41467-024-45957-x, 2024.
868 Choat, B., Brodribb, T. J., Brodersen, C. R., Duursma, R. A., Lopez, R., and Medlyn,
869 B. E.: Triggers of tree mortality under drought, Nature, 558, 531 – 539,
870 https://doi.org/10.1038/s41586-018-0240-x, 2018.
871 Fan, X., Qu, Y., Zhang, J., and Bai, E.: China's vegetation restoration programs
872 accelerated vegetation greening on the Loess Plateau, Agric. For. Meteorol., 350,
873 109994, https://doi.org/10.1016/j.agrformet.2024.109994, 2024.

https://doi.org/10.5194/egusphere-2026-3094
Preprint. Discussion started: 23 June 2026

874 Farquhar, G. D., von Caemmerer, S., and Berry, J. A.: A biochemical model of
875 photosynthetic CO_2 assimilation in leaves of C_3 species, Planta, 149, 78 – 90,
876 https://doi.org/10.1007/BF00386231, 1980.
877 Feng, X., Fu, B., Piao, S. L., Wang, S., Ciais, P., Zeng, Z. Z., Lü, Y. H., Zeng, Y., Li, Y.,
878 Jiang, X. H., and Wu, B. F.: Revegetation in China's Loess Plateau is approaching
879 sustainable water resource limits, Nat. Clim. Change, 6, 1019 – 1022,
880 https://doi.org/10.1038/nclimate3092, 2016.
881 Gong, E. J., Zhang, J., Bai, T. H., Wang, Z. H., Bai, H. Y., and Wang, J.: Spatiotemporal
882 dynamics and influencing factors of precipitation and soil water use efficiency on
883 the Chinese Loess Plateau, J. Hydrol., 644, 134600,
884 https://doi.org/10.1016/j.jhydrol.2025.134600, 2026.
885 Granier, A.: Evaluation of transpiration in a Douglas-fir stand by means of sap flow
886 measurements, Tree Physiol., 3, 309 – 320,
887 https://doi.org/10.1093/treephys/3.4.309, 1987.
888 He, L., Wang, J., Peñuelas, J., Zohner, C. M., Crowther, T. W., Fu, Y. S., Zhang, W. X.,
889 Xiao, J. F., Liu, Z. F., Wang, X. F., Li, J. H., Li, X. J., Peng, S. Z., Xie, Y. W., Ye,
890 J. S., Zhou, C. H., and Li, Z. L.: Asymmetric temperature effect on leaf senescence
891 and its control on ecosystem productivity, PNAS Nexus, 3, 477,
892 https://doi.org/10.1093/pnasnexus/pgae477, 2024.
893 Huang, M. B., Zettl, J. D., Barbour, S. L., Elshorbagy, A., and Si, B. C.: The impact of
894 soil moisture availability on forest growth indices for variably layered coarse-
895 textured soils, Ecohydrology, 6, 214 – 227, https://doi.org/10.1002/eco.1260,

https://doi.org/10.5194/egusphere-2026-3094
Preprint. Discussion started: 23 June 2026

2013.

Jia, X. X., Shao, M. A., Zhu, Y. J., and Luo, Y.: Soil moisture decline due to afforestation across the Loess Plateau, China, J. Hydrol., 546, 113 – 122, https://doi.org/10.1016/j.jhydrol.2017.01.011, 2017.

Jia, X. X., Shao, M. A., Yu, D., Zhang, Y., and Binley, A.: Spatial variations in soil-water carrying capacity of three typical revegetation species on the Loess Plateau, China, Agric. Ecosyst. Environ., 273, 25 – 35, https://doi.org/10.1016/j.agee.2018.12.008, 2019.

Jiao, W., Wang, L., Smith, W. K., Chang, Q., and D'Odorico, P.: Observed increasing water constraint on vegetation growth over the last three decades, Nat. Commun., 12, 3777, https://doi.org/10.1038/s41467-021-24016-9, 2021.

Joshi, J., Stocker, B. D., Hofhansl, F., Zhou, S., Dieckmann, U., and Prentice, I. C.: Towards a unified theory of plant photosynthesis and hydraulics, Nat. Plants, 8, 1304 – 1316, https://doi.org/10.1038/s41477-022-01244-5, 2022.

Kellomäki, S. and Wang, K. Y.: Effects of elevated O_3 and CO_2 concentrations on photosynthesis and stomatal conductance in Scots pine, Plant Cell Environ., 20, 995 – 1006, https://doi.org/10.1111/j.1365-3040.1997.tb00676.x, 1997.

Kengo, O., Yoshiyuki, M., and Daisuke, S.: Rapid stomatal closure contributes to higher water use efficiency in major C_4 compared to C_3 Poaceae crops, Plant Physiol., 189, 188 – 203, https://doi.org/10.1093/plphys/kiac040, 2022.

Li, C., Fu, B., Wang, S., Stringer, L. C., Wang, Y., Li, Z., Liu, Y., and Zhou, W.: Drivers and impacts of changes in China's drylands, Nat. Rev. Earth Environ., 2, 858 –

https://doi.org/10.5194/egusphere-2026-3094
Preprint. Discussion started: 23 June 2026

873, https://doi.org/10.1038/s43017-021-00226-z, 2021.

Li, Q., Yue, Y. M., Wang, L., and Wang, K. L.: Regional differences in carbon-water dynamics of various plantation forests in Southwest China, J. Hydrol., 661, 133809, https://doi.org/10.1016/j.jhydrol.2025.133809, 2025.

Li, Z., Sun, F., Wang, H., and Wang, T.: Declining contribution of plant physiological effects to global drought characteristics with rising CO_2 using state-of-the-art earth system models, Earth's Future, 13, e2024EF005548, https://doi.org/10.1029/2024EF005548, 2025.

Liu, K., Li, X., Li, X. K., Wang, S. D., and Zhou, G. S.: Past and future adverse response of terrestrial water storages to increased vegetation growth in drylands, npj Clim. Atmos. Sci., 6, 113, https://doi.org/10.1038/s41612-023-00437-9, 2023.

Liu, J., Ma, X., Duan, Z., Jiang, J., Reichstein, M., and Jung, M.: Impact of temporal precipitation variability on ecosystem productivity, Water, 7, e1481, https://doi.org/10.1002/wat2.1481, 2020.

Lu, C., Zhang, Q., Woolway, R. I., Ma, L., Liu, T. X., Wang, G., Sun, D. L., Singh, V. P., Bai, Y. G., Sun, B. S., and Huang, X.: Global warming will increase the risk of water shortage in northwest China, Earth's Future, 13, e2025EF006199, https://doi.org/10.1029/2025EF006199, 2025.

Ma, Q., Su, Y., Niu, C., Hu, T. Y., Luo, X. Z., Tai, X. N., Qiu, T., Yao, Z., Bales, R. C., Liu, L. L., Kelly, M., and Guo, Q. H.: Tree mortality during long-term droughts is lower in structurally complex forest stands, Nat. Commun., 14, 7467, https://doi.org/10.1038/s41467-023-43083-8, 2023.

https://doi.org/10.5194/egusphere-2026-3094
Preprint. Discussion started: 23 June 2026

940 Mantova, M., Herbette, S., Cochard, H., and Torres-Ruiz, J. M.: Hydraulic failure and
941 tree mortality: from correlation to causation, Trends Plant Sci., 27, 335 – 345,
942 https://doi.org/10.1016/j.tplants.2021.10.003, 2022.
943 McDowell, N. G., Fisher, R. A., Xu, C. G., Domec, J. C., Hölttä, T., Mackay, D. S.,
944 Sperry, J. S., Boutz, A., Dickman, L., Gehres, N., Limousin, M. J., Macalady, A.,
945 Martínez-Vilalta, J., Mencuccini, M., Plaut, J. A., Ogée, J., Pangle, R. E., Rasse,
946 D. P., Ryan, M. G., Sevanto, S., Waring, R. H., Williams, A. P., Yepez, E. A., and
947 Pockman, W. T.: Evaluating theories of drought-induced vegetation mortality
948 using a multimodel – experiment framework, New Phytol., 200, 304 – 321,
949 https://doi.org/10.1111/nph.12465, 2013.
950 McDowell, N. G., Sapes, G., Pivovaroff, A., Adams, H. D., Allen, C. D., Anderegg, W.
951 R. L., Arend, M., Breshears, D. D., Brodribb, T., Choat, B., Cochard, H., Cáceres,
952 M. D., Kauwe, M. G. D., Grossiord, C., Hammond, W. M., Hartmann, H., Hoch,
953 G., Kahmen, A., Klein, T., Mackay, D. S., Mantova, M., Martínez-Vilalta, J.,
954 Medlyn, B. E., Mencuccini, M., Nardini, A., Oliveira, R. S., Anna, S., Tissue, D.
955 T., Torres-Ruiz, J. M., Trowbridge, A. M., Trugman, A. T., Wiley, E., and Xu, C.
956 G.: Mechanisms of woody-plant mortality under rising drought, CO_2 and vapour
957 pressure deficit, Nat. Rev. Earth Environ., 3, 294 – 308,
958 https://doi.org/10.1038/s43017-022-00272-1, 2022.
959 McDowell, N. G., Pockman, W. T., Allen, C. D., Breshears, D. D., Cobb, N., Kolb, T.,
960 Plaut, J., Sperry, J., West, A., Williams, D. G., and Yepez, E. A.: Mechanisms of
961 plant survival and mortality during drought: Why do some plants survive while

https://doi.org/10.5194/egusphere-2026-3094
Preprint. Discussion started: 23 June 2026

others succumb to drought?, New Phytol., 178, 719 – 739, https://doi.org/10.1111/j.1469-8137.2008.02436.x, 2008.

Melnikova, L., Ciais, P., Boucher, O., and Tanaka, K.: Assessing carbon cycle projections from complex and simple models under SSP scenarios, Clim. Change, 176, 168, https://doi.org/10.1007/s10584-023-03639-5, 2023.

Ouyang, S., Wang, X., Wu, Y. L., and Sun, J. X.: Contrasting responses of net primary productivity to inter-annual variability and changes of climate among three forest types in northern China, J. Plant Ecol., 7, 309 – 320, https://doi.org/10.1093/jpe/rtt066, 2014.

Piao, S. L., Wang, X. H., Park, T., Chen, C., Lian, X., He, Y., Jarle, W. B., Chen, A. P., Ciais, P., Tømmervik, H., Ramakrishna, R. N., and Ranga, B. M.: Characteristics, drivers and feedbacks of global greening, Nat. Rev. Earth Environ., 1, 14 – 27, https://doi.org/10.1038/s43017-019-0001-x, 2020.

Pietsch, S. A., Hasenauer, H., and Thornton, P. E.: BGC-model parameters for tree species growing in central European forests, For. Ecol. Manage., 211, 264 – 295, https://doi.org/10.1016/j.foreco.2005.02.046, 2005.

Qi, G., Song, J., Chen, S., Gong, Y., Bai, H., She, D., and Fu, Y. H.: Increasing impacts of compound extreme droughts on vegetation productivity in China, J. Hydrol., 660B, 133447, https://doi.org/10.1016/j.jhydrol.2025.133447, 2025.

Song, L. N., Zhu, J. J., Zheng, X., Li, X. J. Y., Wang, K., Zhang, J. X., Wang, G. C., and Sun, H. H.: Water use dynamics of trees in a Pinus tabuliformis plantation in semiarid sandy regions, Northeast China, Agric. Water Manage., 275, 107995,

https://doi.org/10.5194/egusphere-2026-3094
Preprint. Discussion started: 23 June 2026

https://doi.org/10.1016/j.agwat.2022.107995, 2023.

Sperry, J. S., Donnelly, J. R., and Tyree, M. T.: A method for measuring hydraulic conductivity and embolism in xylem, Plant Cell Environ., 11, 35 – 40, https://doi.org/10.1111/j.1365-3040.1988.tb01774.x, 1988.

Sperry, J. S., Wang, Y., Wolfe, B. T., Mackay, D. S., Anderegg, W. R. L., McDowell, N. G., and Pockman, W. T.: Pragmatic hydraulic theory predicts stomatal responses to climatic water deficits, New Phytol., 212, 577 – 589, https://doi.org/10.1111/nph.14059, 2016.

Sperry, J. S., Venturas, M. D., Todd, H. N., Trugman, A. T., Anderegg, W. R. L., Wang, Y., and Tai, X.: The impact of rising CO_2 and acclimation on the response of US forests to global warming, Proc. Natl. Acad. Sci., 116, 25734 – 25744, https://doi.org/10.1073/pnas.1913072116, 2019.

Tai, X., Mackay, D. S., Sperry, J. S., Brooks, P., Anderegg, W. R. L., Flanagan, L. B., Rood, S. B., and Hopkinson, C.: Distributed plant hydraulic and hydrological modeling to understand the susceptibility of riparian woodland trees to drought-induced mortality, Water Resour. Res., 54, 4901 – 4915, https://doi.org/10.1029/2018WR022801, 2018.

Tang, Q. and Chen, D.: Global change exacerbates water cycle imbalances and intensifies water resource crises, Sci. China Earth Sci., 68, 3077 – 3080, https://doi.org/10.1007/s11430-025-1661-5, 2025.

Tang, Z., Miralles, D. G., Guo, Z., and Maes, W. H.: Fast response of satellite fluorescence-derived plant physiology to drought stress, Nat. Commun., 17, 2886,

https://doi.org/10.5194/egusphere-2026-3094
Preprint. Discussion started: 23 June 2026

https://doi.org/10.1038/s41467-026-70076-0, 2026.

Thornton, P. E., Law, B. E., Gholz, H. L., Clark, K. L., Falge, E., Ellsworth, D. S., Goldstein, A. H., Monson, R. K., Hollinger, D., Falk, M., Chen, J., and Sparks, J. P.: Modeling and measuring the effects of disturbance history and climate on carbon and water budgets in evergreen needleleaf forests, Agric. For. Meteorol., 113, 185 – 222, https://doi.org/10.1016/S0168-1923(02)00108-9, 2002.

Thrasher, B., Wang, W. L., Michaelis, A., Melton, F., Lee, T., and Nemani, R.: NASA Global Daily Downscaled Projections, CMIP6, Sci. Data, 9, 262, https://doi.org/10.1038/s41597-022-01393-4, 2022.

Torres-Ruiz, J. M., Cochard, H., Delzon, S., Boivin, T., Burlett, R., Cailleret, M., Corso, D., Delmas, C. E. L., De Caceres, M., Diaz-Espejo, A., Fernández-Conradi, P., Guillemot, J., Lamarque, L. J., Limousin, J., Mantova, M., Mencuccini, M., Morin, X., Pimont, F., Dios, V. R. D., Ruffault, J., Trueba, S., and Martin-StPaul, N. K.: Plant hydraulics at the heart of plant, crops and ecosystem functions in the face of climate change, New Phytol., 241, 984 – 999, https://doi.org/10.1111/nph.19463, 2024.

van Genuchten, M. T.: A closed-form equation for predicting the hydraulic conductivity of unsaturated soils, Soil Sci. Soc. Am. J., 44, 892 – 898, https://doi.org/10.2136/sssaj1980.03615995004400050002x, 1980.

Walker, A. P., De Kauwe, M. G., Bastos, A., Belmecheri, S., Georgiou, K., Keeling, R. F., McMahon, S. M., Medlyn, B. E., Moore, D. J. P., Norby, R. J., Zaehle, S., Anderson-Teixeira, K. J., Battipaglia, G., Brienen, R. J. W., Cabugao, K. G.,

https://doi.org/10.5194/egusphere-2026-3094
Preprint. Discussion started: 23 June 2026

Cailleret, M., Campbell, E., Canadell, J. G., Ciais, P., Craig, M. E., Ellsworth, D. S., Farquhar, G. D., Fatichi, S., Fisher, J. B., Frank, D. C., Graven, H., Gu, L., Haverd, V., Heilman, K., Heimann, M., Hungate, B. A., Iversen, C. M., Joos, F., Jiang, M., Keenan, T. F., Knauer, J., Körner, C., Leshyk, V. O., Leuzinger, S., Liu, Y., MacBean, N., Malhi, Y., McVicar, T. R., Penuelas, J., Pongratz, J., Powell, A. S., Riutta, T., Sabot, M. E. B., Schleucher, J., Sitch, S., Smith, W. K., Sulman, B., Taylor, B., Terrer, C., Torn, M. S., Treseder, K. K., Trugman, A. T., Trumbore, S. E., van Mantgem, P. J., Voelker, S. L., Whelan, M. E., and Zuidema, P. A.: Integrating the evidence for a terrestrial carbon sink caused by increasing atmospheric CO_2, New Phytol., 229, 2413 – 2445, https://doi.org/10.1111/nph.16866, 2021.

Wang, F., Zhang, J. Z., Fonti, P., Sun, Q. P., Wang, Y. T., Zhang, F., Wang, Y. F., Yang, J. Q., and Gou, X. H.: Effects of site aridity and species on stand transpiration in high-elevation dryland ecosystems, J. Hydrol., 630, 130662, https://doi.org/10.1016/j.jhydrol.2024.130662, 2024.

Wang, L. N.: Loess Plateau Chinese pine plantation drought risk assessment, Doctoral dissertation, Beijing Forestry University, 2016.

Wang, M. J., Peng, S. S., Lu, Z. H., Xu, X. T., Felton, A., and Chen, A. P.: Increasing constraint of aridity on tree intrinsic water use efficiency, Nat. Commun., 16, 7560, https://doi.org/10.1038/s41467-025-62845-0, 2025.

Wang, Z., Liu, B., Liu, G., and Zhang, Y. X.: Soil water depletion depth by planted vegetation on the Loess Plateau, Sci. China Ser. D-Earth Sci., 52, 835 – 842,

https://doi.org/10.5194/egusphere-2026-3094
Preprint. Discussion started: 23 June 2026

https://doi.org/10.1007/s11430-009-0087-y, 2009.

Wolfe, B. T., Sperry, J. S., and Kursar, T. A.: Does leaf shedding protect stems from cavitation during seasonal droughts? A test of the hydraulic fuse hypothesis, New Phytol., 212, 1007 – 1018, https://doi.org/10.1111/nph.14087, 2016.

Wu, X. F., Yan, X. Y., Zhang, Z. D., Huang, M. B., Liu, X. M., and Guo, T. Q.: Differences in actual evapotranspiration and responses of pure and mixed forests to climate change on the Chinese Loess Plateau, Agric. For. Meteorol., 385, 111210, https://doi.org/10.1016/j.agrformet.2026.111210, 2026.

Xu, F., Qu, Y., Bento, V. A., Song, H. Q., Qiu, J. X., Qi, J. Y., Wan, L. L., Zhang, R. R., Miao, L. J., Zhang, X. S., and Wang, Q. F.: Understanding climate change impacts on drought in China over the 21st century: a multi-model assessment from CMIP6, npj Clim. Atmos. Sci., 7, 32, https://doi.org/10.1038/s41612-024-00578-5, 2024.

Yan, X. Y., Zhang, Z. D., Huang, M. B., Zhao, X. F., Yang, F., and Wu, X. F.: The impact of climate change on growth and drought-induced mortality risk of Robinia pseudoacacia plantations along a precipitation gradient on the Chinese Loess Plateau, Agric. For. Meteorol., 325, 109160, https://doi.org/10.1016/j.agrformet.2022.109160, 2022.

Yang, K. Q., Ma, Z. H., Wang, K., Li, G. L., Zhang, X. Y., Zhen, Q., and Zheng, J. Y.: Combining infiltration hole and mulching techniques with fish-scale pits effectively improved soil water storage in semiarid areas with shallow buried bedrock (Pisha Sandstone) in China, Catena, 230, 107249, https://doi.org/10.1016/j.catena.2023.107249, 2023.

https://doi.org/10.5194/egusphere-2026-3094
Preprint. Discussion started: 23 June 2026

1072 Zhang, Z. D., Jia, X. X., Zhu, P., Huang, M. B., Ren, L. D., and Shao, M. A.: Estimating
1073 the optimal vegetation coverage for the dominant tree and shrub species over
1074 China's northwest drylands, Sci. China Earth Sci., 67, 1500 – 1517,
1075 https://doi.org/10.1007/s11430-023-1287-x, 2024a.
1076 Zhang, Z. D., Liu, T. H., Huang, M. B., Yan, X. Y., Liu, M. H., Yan, J. H., Chen, F. Y.,
1077 Yan, W., and Niu, J. Q.: Spatial pattern of drought-induced mortality risk and
1078 influencing factors for Robinia pseudoacacia L. plantations on the Chinese Loess
1079 Plateau, Forests, 15, 1477, https://doi.org/10.3390/f15081477, 2024b.
1080 Zhang, Z. D., Huang, M. B., Yang, Y. N., and Zhao, X. F.: Evaluating drought-induced
1081 mortality risk for Robinia pseudoacacia plantations along the precipitation
1082 gradient on the Chinese Loess Plateau, Agric. For. Meteorol., 284, 107897,
1083 https://doi.org/10.1016/j.agrformet.2019.107897, 2020.
1084 Zhou, G. Y., Yi, G. C., and Tang, X. L.: Forest Ecosystem Carbon Stocks in China –
1085 Biomass Equations, Science Press, Beijing, 44 pp., ISBN 9787508853925, 2018.
1086 Zhou, S., Williams, A. P., Berg, A. M., Cook, B. I., Zhang, Y., Hagemann, S., Lorenz,
1087 R., Seneviratne, S. I., and Gentine, P.: Land – atmosphere feedbacks exacerbate
1088 concurrent soil drought and atmospheric aridity, Proc. Natl. Acad. Sci., 116,
1089 18848 – 18853, https://doi.org/10.1073/pnas.1904955116, 2019.
1090 Zhu, Y. J., Jia, X. X., and Shao, M. A.: Loess thickness variations across the Loess
1091 Plateau of China, Surv. Geophys., 39, 715 – 727, https://doi.org/10.1007/s10712-
1092 018-9462-6, 2018.